IEEE Access
Multidisciplinary | Rapid Review | Open Access Journal

Received July 27, 2021, accepted August 23, 2021, date of publication September 13, 2021, date of current version September 29, 2021.

Digital Object Identifier 10.1109/ACCESS.2021.3112297

Machine Learning Assisted Visible Light Sensing of the Rotation of a Robotic Arm

KUSHAL MADANE[1], ANDREAS PETER WEISS[1], STEFAN SCHANTL[1], ERICH LEITGEB[2], (Member, IEEE), AND FRANZ PETER WENZL[1]

[1]MATERIALS–Institute for Surface Technologies and Photonics, JOANNEUM RESEARCH Forschungsgesellschaft mbH, 7423 Pinkafeld, Austria
[2]Institute of Microwave and Photonic Engineering, Graz University of Technology, 8010 Graz, Austria

Corresponding author: Franz Peter Wenzl (franz-peter.wenzl@joanneum.at)

This work was support by the Austrian Bundesministerium für Klimaschutz, Umwelt, Energie, Mobilität, Innovation und Technologie (BMK), project "HIGH-Light."

ABSTRACT With the rise of LED (light-emitting diode)-based luminaires, artificial lighting has become a technology platform, which, besides providing illumination, also provides communication and positioning functionalities. Apart from this, most recently Visible Light Sensing (VLS), in which lighting is used for sensing purposes, emerged as another embodiment of functionalities lighting could take over in the future. Here we show that machine learning assisted VLS has promising potentials to become a meaningful enabler for the Industrial Internet of Things. We show that the rotation of a robotic arm can be accurately monitored by VLS simply by equipping the robotic arm with sequences of colored retroreflective foils. Moreover, we show that the sensing task is compatible with a modulation of the light. This paths the way that sensing and communication tasks can be performed in parallel with one and the same low-complexity infrastructure, that apart from this also could take over the task of the obligatory room lighting. We demonstrate the capability of the approach even if the overall illumination conditions change. Therewith, VLS accentuates as an alternative option for industrial robot monitoring in combination with optical wireless communication.

INDEX TERMS Lighting, visible light communication, visible light sensing, machine learning, Industry 4.0.

I. INTRODUCTION

With the invention of LED-based lighting [1]–[3], artificial lighting has evolved from a simple provider of illumination to a technology platform that, based on its ability of controlling light intensity and spectral power distribution, allows to consider also non-visual effects of light, which can support the physiological behavior of humans, plants or animals [4]. Other functionalities that gained more and more interest during the last years rely on the use of artificial lighting for communication and positioning tasks, commonly referred to as Visible Light Communication (VLC) and Visible Light Positioning (VLP) [5]–[9]. VLC provides illumination and communication at the same time [10] and takes advantage from the possibility of LED-based luminaires to encode data into light intensity modulations with frequencies that are beyond the flicker perception level of humans [11]. A receiver, typically a photodiode, again records these modulations. Furthermore, VLC distinguishes by a high bandwidth, immunity to Radio frequency (RF)-based interferences and its low latency. VLP has also promising capabilities, which can be used for indoor positioning, where systems like the Global Positioning System (GPS) are less effective. Different techniques, such as Triangulation, Fingerprinting, Angle of Arrival and so on, can be used to determine the position of a receiving object accurately [12].

Most recently, another functionality, which uses the same infrastructure as VLC and VLP, gained notable momentum: (backscattered) visible light sensing (VLS) [13]. VLS relies on the analysis of the reflected light from an object or a surface. To extend the potentials of VLS, these surfaces can be coated with codes, this means sequences of surface areas with different reflectivity values or different colors. This supports the identification of an object, its position or a movement of the object [14], [15]. Applications of VLS range from presence detection [16], pose detection [17] occupancy estimation [18], and hand gesture recognition [19], [20] to vital sign monitoring [21]. Especially in scenarios in which human beings are involved, VLS has the advantage that it does not cause privacy concerns. Moreover, the implementation

The associate editor coordinating the review of this manuscript and approving it for publication was Chunsheng Zhu.

of VLS does not necessitate notable effort since it can be easily integrated into the obligatory lighting infrastructure.

The concepts of VLC [22] and VLP [23] still have found their ways into considerations to support the needs of Industry 4.0 and the Industrial Internet of Things (IIoT) [24]–[28]. For instance, the large number of devices that have to be controlled and coordinated in IIoT, pose some problems for RF wireless communication, in particular problems with interference and spectrum limitations [25]. Because of the progress of VLC in the last years, the International Telecommunication Union has identified it as a mature technology for offloading the RF spectrum [29].

In the following, we demonstrate the promising role VLS could play in future IIoT applications in addition to VLC by discussing its ability to determine the rotation of a robotic arm on the base of machine learning (ML) approaches. We name this combination of machine learning and VLS as machine learning assisted VLS. The corresponding experimental set-up is shown in Figure 1.

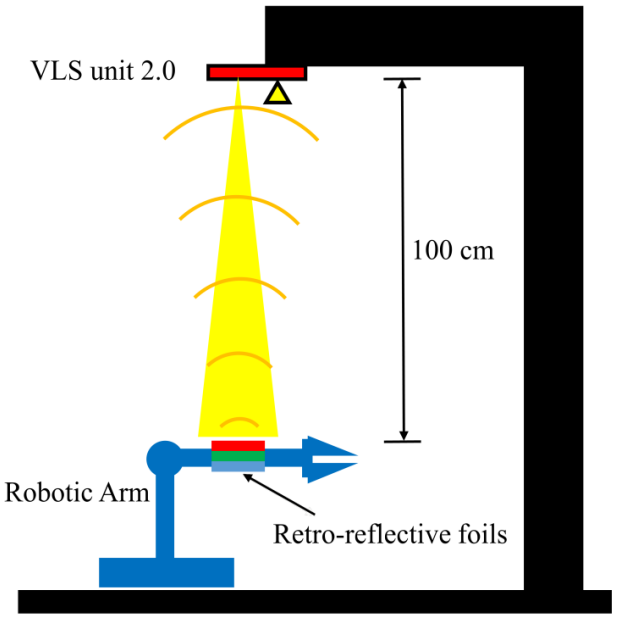

FIGURE 1. Overall sketch of the experimental set-up.

An LED mounted on a printed circuit board (PCB), which is a part of the VLS unit 2.0 (see later), illuminates a robotic arm. The robotic arm is equipped with a sequence of three or more retroreflective foils of different colors. Eight colored retroreflective foils named 3M_Red, 3M_Green, 3M_Blue, 3M_Yellow, 3M_White, Ora_Red, Ora_Yellow and Ora_White are used for this study [30], [31]. The abbreviations Ora and 3M in the foil names refer to their manufacturers, 3M and Orafol respectively. Some portion of the light that is reflected from these foils impinges on a photodiode that is also mounted on the same PCB, nearby the LED.

In addition, we demonstrate that the light used for illuminating the robotic arm for sensing purposes can also be modulated in parallel. This means that such an approach has the potential to communicate with the robotic arm by VLC and in parallel sense its motion by VLS, using the same infrastructure.

Such a system would have tremendous potential in industrial environment applications where robotic arms are very frequently used. In our work, we will show that our proposed solution can overcome some of the problems on the horizon for IIoT applications by establishing a system, where no active sensors on the robotic arm for motion detection and control are necessary. Furthermore, we will show that by combining the VLS task of sensing the rotation of the robotic arm with the functionality of data transmission by the means of VLC, an RF-free infrastructure is introduced, which allows to avoid the before mentioned problems with interferences and spectrum limitations predicted for RF communication in future. We will additionally show that with machine learning assisted VLS, a system that requires only minimal training effort for the ML model generation can be established, that facilitates high accuracies in the determination of the rotation of the robotic arm. With the experimental data presented in this work we will demonstrate that our solution approach is also resilient against environmental changes (e.g. additional ambient light) to a notable extend, without the need for repeating the training phase.

II. SOLUTION APPROACH

In many applications, such as activity recognition, localization or movement detection, machine learning (ML) algorithms are nowadays widely used [32].

Key factors that determine the achievable results as well as the overall complexity are the feature selection and the amount and quality of the required training data. In this regard, a ''feature'' means a measureable value of a situation or an event, e.g. sensor readings or calculated values based on sensor readings.

The term ''training data'' describes an aggregation of such features that are used to generate a model of the underlying scenario. The established model predicts the outcome in case that new and unknown data are added to the model. Supervised learning algorithms, which are a subset within the broad range of available ML algorithms, generally yield good results [33], whilst rendering low computational complexity.

In the field of supervised learning algorithms, decision tree algorithms are a suitable choice for implementations in the industrial area, because their structure favors a direct implementation in source codes. Since modeling of the training data is a difficult and time-consuming task, the way in which the training data are generated is one of the key aspects in applying ML for movement detection.

One approach for modeling movements in the training data would be to apply time-domain and/or frequency domain methods to generate features that map out the characteristics of the respective movements. In [34], it is shown

how different activities such as walking, sit-to-stand, etc., performed by a human being and measured with Inertial Measurement Unit (IMU) sensors can be detected with such time- and/or frequency domain methods. When applying such an approach, the generation of the training data is a complex task since every variation of the scenario, such as different walking speeds, etc., has to be trained separately in order to generate a meaningful training phase. Conferred to our scenario at hand, which is the detection of the rotation of a robotic arm equipped with retroreflective foils of different size and color configurations, this would lead to the very time-consuming task of training all potential scenarios for all applicable speeds and all directions (clockwise/counterclockwise) of potential robotic arm rotations. Substituting for example only one foil of the sequence would result in the necessity to redo the complete training procedure again.

Our solution approach in this regard is based on the theorem that, although a movement occurs, during the movement, phases for which only one foil is reflecting the light back to the VLS unit 2.0 can be determined. When only one foil is reflecting the light back, we reason that this foil can be determined accurately based on the spectral composition of the light impinging on the photodiode. It is clear that during the movement for a certain time-period multiple foils will reflect light back to the VLS unit 2.0 and therefore the impinging light will be a mixture of the reflections from multiple foils. We name such a time-period during which light from multiple foils is reflected toward the photodiode a transition period. This leads to the second theorem of our approach, that these transition periods, although unavoidable, can be filtered out and consequently the resulting sequence of detected foils is a series of phases in which only one foil is reflecting the light back to the VLS unit 2.0.

With these assumptions, we infer that the training effort will be minimal since we do not train with respect to time-dependent data, but merely with respect to the reflected light, which is a similar approach to the one we presented in [35]. Due to the fact, that there is no time-dependency in the training data, we can infer the following:

- The sequences of the foils placed on the robotic arm will not deteriorate the results
- The detection of the foils will not depend on the speed of the movement.
- The direction of the movement (clockwise/counterclockwise) will not affect the achievable results.

In the following, we will show the applicability of our approach for various scenarios, such as differently colored foils placed on the robotic arm, a varying number of foils, diverse rotational speed values as well as the resilience of our system against ambient light and a tilt of the robotic arm. Finally, we will also show that the incorporation of a modulation of the light source in order to enable VLC in parallel does not interfere with the task of the rotation detection and its accuracy. A graphical overview of the proposed solution approach and its integral parts is given in Figure 2.

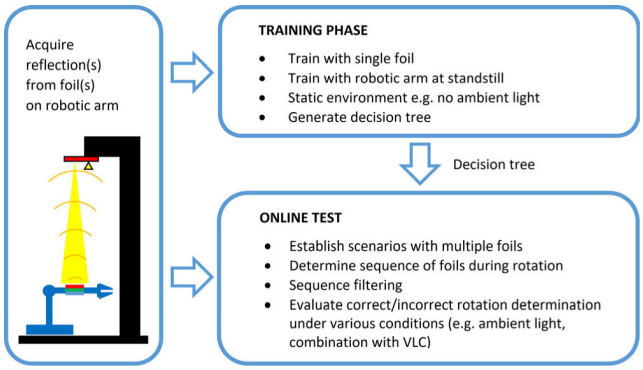

FIGURE 2. Overview of proposed solution approach.

III. VLS UNIT 2.0

An industrial environment poses several challenges for applications in the domains of VLS and VLC. For the design of such systems, aspects such as robustness, size, low maintenance effort, low-complexity and low-cost for both hardware and software as well as the necessary installation effort regarding supply voltages, backend communication, etc., must be taken into account. Furthermore, aspects to guarantee precise synchronization between multiple of such nodes must be also considered already in the design phase. Considering all these requirements, a VLS unit 2.0, which is an enhancement of the VLS unit discussed in [35], was designed to fulfill these challenging requirements.

The VLS unit 2.0 consists of two main components, an Ultra96-V2 board of the vendor AVNET Inc. [36] and a self-developed PCB establishing an optimized analog frontend as well as the Analog to Digital conversion stage. This self-developed PCB design is named PCB board in the following. A detailed description of this analog frontend is given in sections A and B of this chapter.

The chosen Ultra96-V2 board relies on an Arm-based, Xilinx Zynq UltraScale+^{TM} MPSoC processing unit. This development board has a small form factor (85 mm $\times$ 54 mm) and offers multiple built-in communication interfaces (WiFi, USB, Ethernet etc.) amongst other functionalities, for further details please see [37]. The main advantage of utilizing an MPSoC platform is that whilst all time-critical aspects of the system, such as Analog-to-Digital converter (ADC) control, etc., can be implemented in the FPGA part of the processing unit, all functionalities with lower time-dependency can be implemented in the System-on-a-chip (SoC) part. In the SoC part, all the advantages of having the possibility of using higher-level programming languages (e.g. C) as well as higher-level access to the peripherals can be exploited. The possibility of assigning certain tasks to the two parts of the processing unit is a huge benefit of the system, whilst keeping the software implementation effort small.

Our in-house developed analog frontend (PCB board), which is directly attachable to the Ultra96-V2 board as a piggyback extension, contains two main subsystems (see A. and B.) along with other subsidiary parts, such as power rail regulator units, level translators for the LED

driver, an I2C temperature sensor and a MEMS based high-performance 3-axis digital accelerometer, respectively a 3-axis digital gyroscope inertial sensor module. Although, for example, the inertial sensor module is not used in this work, we already can point out that the design is capable of enabling future works also for other VLS application scenarios.

A. TRANSMITTER SUBSYSTEM (LED DRIVER)

The transmitter module is build-up of a CREE RGBW MCE LED [38] and a GaN based LED driver circuit. The LED consists of four separate dies (for Red, Green, Blue and White), which can be controlled individually. For the modulation of the individual LED dies, the EPC2040 GaN power transistor was chosen [39]. This transistor has a small form factor and can handle a high current at high switching frequencies. To control this FET, the LMG1020 GaN low-side gate driver [40] was selected, since it can source and sink a large amount of current to the gate of the FET, which is a requirement for fast rise and fall times at high-speed LED current modulations. The gate driver works with a 5 V logic level. Since the Ultra96-V2 board can only provide a 3.3 V level, an additional voltage level translator was used for conversion. The driver design was done in such a way, that each die can carry 350 mA individually. A current limiting resistor was used to keep the LED current of each die at a maximum of 350 mA. All resistors were chosen with proper wattage class rating to carry 350 mA of current without any thermal issue. An extra heatsink is attached to these resistors to provide a proper thermal design. The input stage of the logic level translator is connected to dedicated General-Purpose Inputs/Outputs (GPIOs) of the Ultra96-V2 board. One channel of the GaN based LED driver module is shown in Figure 3. The GPIOs are part of the FPGA and can be easily controlled via the ARM Cortex of the Xilinx MPSoC. The PCB footprint of the LED was done in such a way, that proper heat dissipation, with a standard heat sink on the bottom side of the PCB, is possible. A temperature sensor was placed close to the LED to monitor the thermal performance of the PCB design. The thermal behavior can be changed with a controllable fan at the heatsink, regulated by a software implemented PID unit.

B. RECEIVER SUBSYSTEM

The receiver module is based on a Kingbright APS5130PD7C-P22 RGB color sensor [41], consisting of a 3-Channel/1Chip (R, G, B) Si photodiode. Each photodiode of this color sensor has its own individual amplifier and data-sampling channel. The weak photocurrents generated by the photodiodes are amplified via transimpedance amplifiers (TIA). LTC6268-10 op-amps [42] from Linear Technology Cooperation were used as transimpedance amplifiers, since this op-amp has very low parasitic capacitance, very low bias current, and a high bandwidth of up to 4 GHz, which enables high switching frequencies. Dark current compensation has been implemented using a second identical color sensor, connected to the respective non-inverting inputs of the operational amplifiers. This second color sensor is covered with a black tape, so that no light impinges at the active area and only dark current is generated. Thus, the offset voltage caused by the dark current of the regular circuit will be cancelled out at the transimpedance amplifier output. The second color sensor is placed right below the main color sensor on the bottom side of the PCB. With this, the lengths of the tracks and the temperatures at the photodiodes are almost the same, which causes them to generate the same dark current and thus helps in canceling out any kind of offset respectively noise at the outputs of the transimpedance amplifiers. Due to the internal build-up of the RGB photodiodes, the outputs of the transimpedance amplifiers are negative and in the range of GND to negative supply (V-) of the op-amp supply voltage.

Extra stages of op-amps are required for inverting the signal back and converting it to a differential one. One stage of the LTC6229 dual op-amp [43] from Analog Devices is used to invert the output signal of the transimpedance amplifier via an inverting amplifier circuit, and pre-amplifies the signal itself. The next op-amp stage, with the same type of op-amps, is used for single-ended to differential conversion of the signal. This op-amp stage, along with a low pass filter, acts as the input driver of the ADC. In Figure 4, the RC low pass filter right before the ADC inputs, along with the complete ADC driver circuit including the transimpedance amplifier of a single channel, is shown.

Each of the three channels was build up in the same way. The ADC used in this circuit is the LTC2387-16 from Linear Technology Cooperation [44] and has analog differential inputs. This ADC has a common-mode output voltage of nominal 2.048 V to set the common-mode of the analog inputs. This common-mode voltage is buffered via the free and unused op-amp of the first LTC6229 op-amp stage. The complete analog ADC design was done in such a way that an analog pulse-switching rate of 100 kHz and data sampling rate of 1 MHz can be achieved.

Communication between the Ultra96-V2 board and the ADCs of the VLS unit 2.0 is done via LVDS signals at 100-ohm differential transmission lines. Positive and negative 5 V rails are provided to the VLS unit 2.0 for smooth operation. Positive and negative 2.5 V rails, needed for the transimpedance amplifiers, are provided from the low noise low dropout linear regulators circuitry included in the PCB design. A 3.3 V power rail, needed for the temperature and the inertial sensors, is obtained directly from the Ultra96-V2 board.

There is also the possibility of powering the entire VLS unit 2.0 from the Ultra96-V2 board via the onboard connectors, but an additional external 5 V supply is needed to power the LEDs and the driver circuit. The raw PCB was manufactured by Wuerth Electronics and the component assembly was done by Astron Electronics Gmbh. A housing for the PCB was fabricated using an in-house 3D printer. It includes holes for fixation to easily mount the complete unit on an aluminum construction, build-up for the experiments. Figure 5 shows the 3D model of the complete VLS unit 2.0 with the 3D

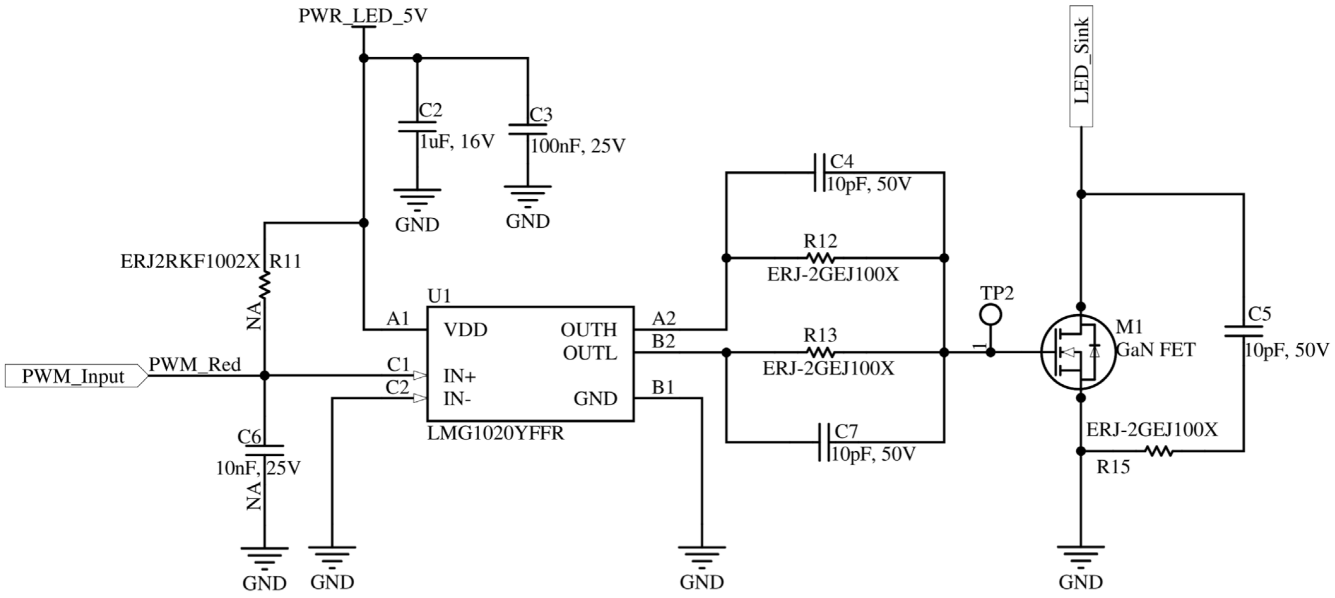

FIGURE 3. Single channel GaN FET-based LED driver circuit.

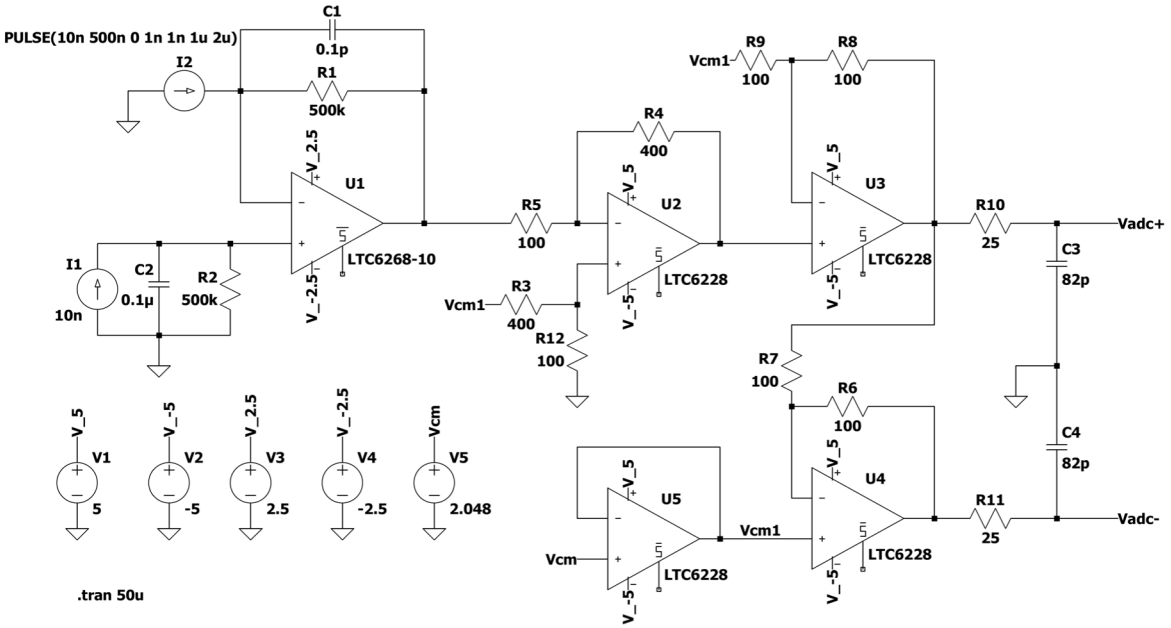

FIGURE 4. ADC driver circuit including transimpedance amplifier.

printed housing. Please note that the Ultra96-V2 board is attached on the bottom side and therefore not visible in the 3D model.

C. FPGA AND SOFTWARE IMPLEMENTATION

Our design approach of utilizing a processing unit that offers an FPGA subsystem for time-critical functionalities alongside a SoC part that supports higher level programming and various easy to access interfaces as outlined before, is also reflected in the assignment of the implemented software to these subsystems.

Most of the control software, such as for LED control, timer implementation for time keeping, thermal control, and decision tree processing is done with the ARM Cortex processor of the Xilinx MPSoC on the Ultra96-V2 Board. We like to point out that in the initial set-up the LED is switched continuously on and therefore the control can be done by the SoC part. Later we will show that in case that the LED is aimed

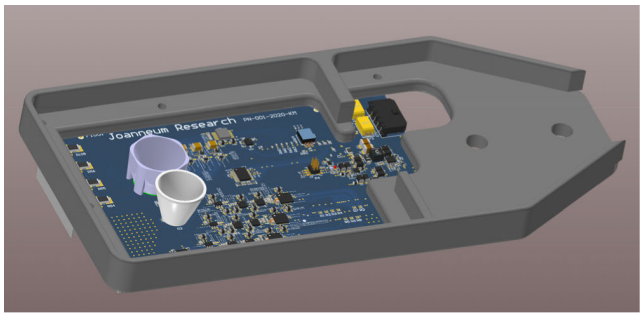

FIGURE 5. 3D model of the VLS unit 2.0 with the 3D printed housing.

to be modulated, this control functionality can be transferred to the FPGA in order to guarantee a precise time behavior. The important peripherals to fetch the data from the ADC, using LVDS signaling, are implemented on the FPGA. The SoC side accesses the ADC data via an implemented AXI bus interface. A shift register is implemented, which stores the serial data from the ADC to a 16-bit AXI register. Each of the three color channels has a separately implemented AXI bus. Figure 6 shows a block diagram of the implemented software components and their assignment to the FPGA respectively the SoC parts, as well as the used interfaces.

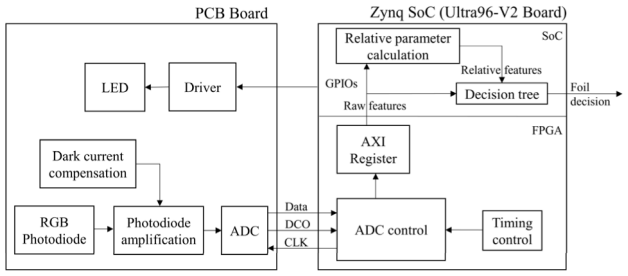

FIGURE 6. Block diagram of the FPGA and SoC implementations and the interfaces between the PCB board and the Ultra96-V2 board.

As shown in Figure 6, the established decision trees as well as necessary calculations to create additional features for the decision trees is done in the SoC part of the processing unit. The process of feature selection and the generation of the decision trees is described in detail in the next section.

IV. FEATURE SELECTION AND DECISION TREE GENERATION

For every machine learning approach the process of feature selection is one of the most crucial tasks. The most straightforward approach in selecting the features to describe a foil is to use the raw values measured with the RGB photodiode for the three color channels, Red, Green and Blue. This means that when a certain foil reflects the light, the RGB photodiode yields certain values. These values are affected by (modifications of) the amount of light that impinges on the foil, the size of the reflective area and the distance between the foil and the VLS unit 2.0. Since we therefore anticipate that utilizing these absolute numbers as features is problematic, we devised an approach where features representing relative characteristics of the reflected light are used. By utilizing relative features, we basically use the spectral composition of the received reflections to characterize a foil instead of raw values. The devised relative features are given in Table 1.

With this easy to calculate relative parameters it is possible to delineate the impinging light without having to rely on absolute numbers. The calculation of the relative features is done in the SoC part of the processing unit. In the Experimental results chapter we will compare the achieved results for a decision tree based on the raw values with the achieved results for a decision tree based solely on the described relative features.

TABLE 1. Relative parameters.

Relative parameter	Calculation from raw values
Red_Green	= Red - Green
Red_Blue	= Red - Blue
Green_Blue	= Green - Blue
Div_Red_Green	= Red ÷ Green
Div_Red_Blue	= Red ÷ Blue
Div_Green_Blue	= Green ÷ Blue

With these two sets of features established, we can generate the decision trees that will perform the task of identifying the foil that is currently reflecting the light towards the VLS unit 2.0. These decision trees are generated using a machine learning-based tool called Waikato Environment for Knowledge Analysis (WEKA) [45]. For this, first, offline data of all the foils are created. These data are stored in the form of a CSV file, which contains all the raw values (raw features), the computed relative features and the label resembling the class needed for the supervised machine learning method of decision trees. To create such a file, the following procedure was undertaken.

First, a foil is placed around the cylindrical area of Joint 4 on the robotic arm. The foil placed on this arm now can be rotated around its axis up to 350 degrees. The area used on the robotic arm where the foil is attached has a width of 5.1 cm while the circumference of the arm is 11 cm. In order to form the training data for this foil the white die of the LED is turned on, and the reflected light from this foil is measured by the VLS unit 2.0 with 5 Hz sampling frequency. As will be discussed later on, one of the advantages of our approach, to not train with respect to time-dependent data, is that the sampling rate utilized during the training phase can differ from the utilized sampling rates during the experiments. Therefore, we deliberately chose a different sample rate for the training phase, compared to the experiments. To account for imperfections of the used foils, the arm was rotated six times and the measurements are repeated. Please note that the measurements were recorded when the arm had reached a standstill, to guarantee that only stable reflections are present.

Overall, by following this procedure for every utilized foil, 2400 datasets (300 datasets per foil) were generated. These datasets contain the raw values from the three ADC

channels and the six relative parameters (Red-Green, Red-Blue, Green-Blue, Red/Green, Red/Blue, Green/Blue). These measurement results were printed on the terminal along with the timestamp and the temperature of the LED lamp for monitoring purposes. The 300 datasets of each foil were then stored in a CSV file with the necessary class identifier, which is the respective foil name. This was repeated for all eight foils and the data were finally concatenated into a single file.

This file was then imported into the WEKA tool and subsequently used to generate the decision trees. By a simple checkbox selection, the features to be used were set. The first decision tree generated used only the raw value based features, whilst the second one utilized the six relative features described earlier. For both of the decision trees, the J48 classifier was used in the WEKA tool. The generated decision trees were stored in a text file. In Figure 7 and Figure 8, the resulting decision trees for the raw features and the relative features are visualized. It is important to emphasize that this process is done only once for each of the foils and does not require any repetition when further on the area on the robotic arm is segmented into multiple foils.

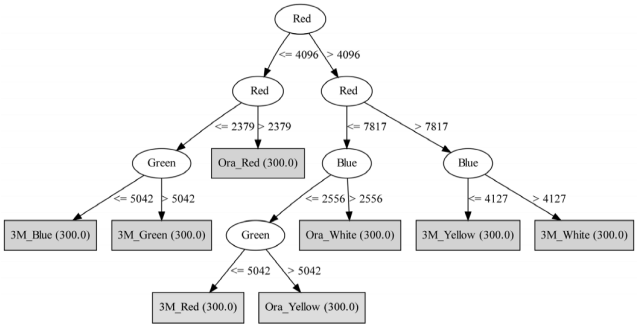

FIGURE 7. Decision tree obtained for the raw features.

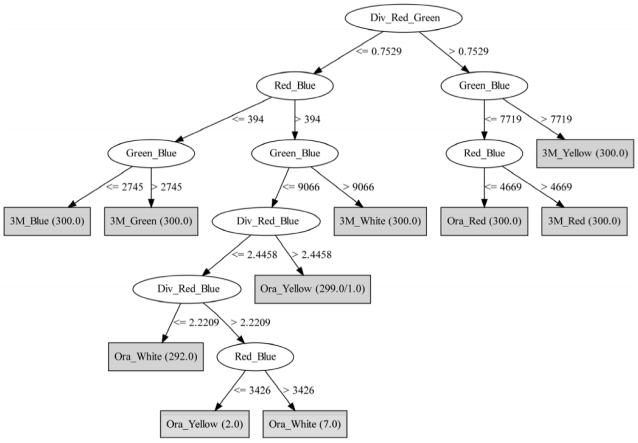

FIGURE 8. Decision tree obtained for the relative features.

The decision trees shown in Figure 7 and Figure 8 were then translated into nested if-statements in C code, thus showing that the implementation can be done in a very straight-forward manner and requires only low technical complexity and low time effort for the realization. As shown in the software/hardware block diagram (Figure 6) the decision trees are implemented in the SoC part of the processing unit. For every measurement, the two trees outputted their decisions, which foil "caused" the respective reflections. This decision was then printed on a terminal window.

V. EXPERIMENTAL SET-UP

The measurement set-up established for our experiments consists of the VLS unit 2.0 mounted on a fixed aluminum construction and a Niryo One robotic arm, from the vendor Niryo [46], placed at a fixed distance on the floor beneath the VLS unit 2.0. Special care was taken that the construction holding the VLS unit 2.0 was reinforced properly and remained immobile during the measurements. The height distance between the VLS unit 2.0 and the area on the robotic arm where the retroreflective foils were placed is 1 m. An external power supply was used to power both elements of this set-up. The set-up was assembled in one of our laboratory rooms, where the shades can be closed completely to block sunlight. In this laboratory room artificial lighting is supplied by 4 luminaires (each holds 2 fluorescent tubes) placed on the ceiling of the room. These luminaires were off during the training and the tests described in chapter VII, except the subchapter VII – I, where the influence of ambient light on the system performance is discussed. The movement of the robotic arm was controlled wirelessly by a Graphical User Interface (GUI) provided by the manufacturer of the robotic arm. The robotic arm has seven joints, out of which Joint '3' and '4' are relevant for our experiments. Joint '4', where the foils are placed, was used to rotate the arm up to 350 degrees around its cylindrical axis. Joint '3' was used to move the arm up to 90 degrees in up and down directions, resulting in a tilt of the reflective area with respect to the plane of the VLS unit 2.0. A black mat was placed under the robotic arm so that the reflections from the floor were minimized. The walls of the laboratory room are painted with white color. The whole set-up was built-up in a corner of the room with no furniture or other objects in the vicinity of the experimental set-up. Figure 9 shows a picture of the final set-up with the main components labelled such as the VLS unit 2.0 and the area on the robotic arm where the retroreflective foils were placed.

A GPIO interface was used to interface between the robotic arm and the VLS unit 2.0, which is a prerequisite in order to process the results effectively. The GPIO signal level was set to '1' for performing a clockwise movement and to '0' for a counterclockwise movement. For the performed measurements only the white die of the LED was turned on, leaving the other three dies of the LED switched off. The illuminance value at the surface of the reflective area was ∼265 lux, measured with a handheld MK350S PREMIUM spectrometer. The temperature of the LED was regulated actively by controlling the FAN PWM mounted on the heat sink of the LED. This was done by implementing a proportional controller in the software that samples the temperature sensor placed close to the LED at 5 Hz. The

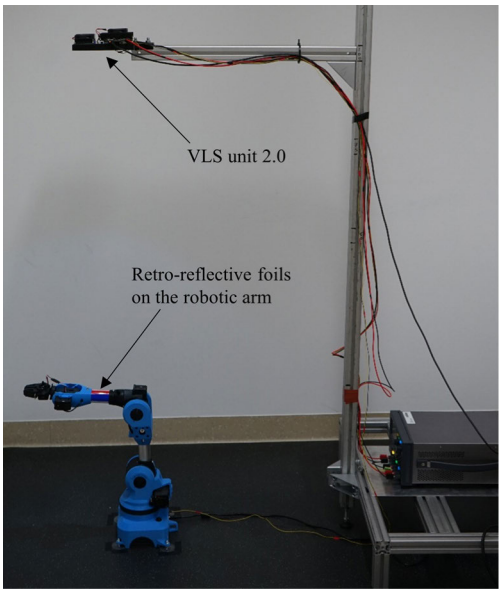

FIGURE 9. Experimental set-up.

set-point of this controller was set at 35 degrees centigrade, but the actual temperature of the LED most probably was higher than this value, since the temperature sensor is placed 5 mm away from the LED. The temperature regulation took around 20 min to reach the stable temperature set-point, and the observed temperatures after stabilization were oscillating within 0.2 degrees from the set-point, which is sufficient to guarantee an almost stable radiant flux from the LED. All the measurements were recorded after temperature stabilization.

VI. MEASUREMENTS

With the generated decision trees (see Figure 7 and Figure 8), based on either the raw values or the computed relative values, the online phase in order to determine the respective foil that faced upward, toward the VLS unit 2.0, was conducted. As described above, the decision trees were implemented in C and performed in the SoC part of the Ultra96-V2 board. The workflow of the measurements can be divided into two independent actions performed by the robotic arm and the VLS unit 2.0.

The robotic arm performed a 350° rotation in either clockwise or counterclockwise direction. As mentioned before, in order to enable the determination if an achieved result is correct or incorrect, the direction of the movement was signaled to the VLS unit 2.0 via a GPIO pin. One 350° rotation is considered as one run of a scenario.

Within the overall workflow, the ADC samples the light impinging on the RGB photodiode after the TIA stages. The acquired raw values were then transferred to the SoC part of the board via the described AXI bus. The raw values were subsequently used on the one hand to calculate the relative parameters and on the other hand were directly supplied to the decision tree utilizing the raw values. After the calculation of the relative parameters, these were also supplied to their respective decision tree, utilizing the relative values as the input. So, for each acquired sample the implemented decision trees outputted which foil was facing upward toward the VLS unit 2.0 as a classification result in each case. The two classification results were then timestamped and displayed on a terminal window along with the status of the GPIO connected to the robotic arm, showing in which direction the movement was performed (clockwise/counterclockwise). This text output of one run was then stored to a text file and processed further on by applying filtering and consequently the assessment, whether the result of this run could be qualified as correct or incorrect, was done. The descriptions of the filtering process and the results assessment are given in chapter VII – subchapter A and subchapter B.

For a better descriptiveness of the following parts, a naming scheme is introduced. The term segmentation means that different retroreflective foils are placed on the robotic arm in identical sizes, subdividing the 11 cm circumference. So, for example, Segmentation type 3 means that the cylindrical shape of the robotic arm is divided into 3M_Red, 3M_Blue and 3M_White foils. Figure 10 shows an image how these foils were placed on the robotic arm. Table 2 summarizes the applied segmentation types, given in the order of a clockwise movement.

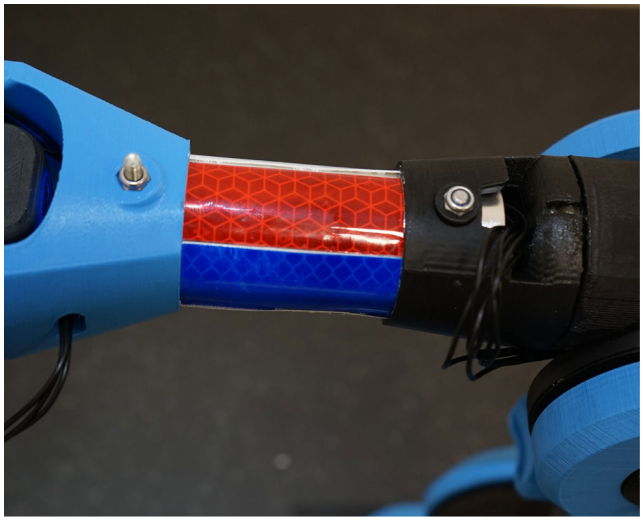

FIGURE 10. Foil segmentation on the robotic arm.

TABLE 2. Foil types and dimensions of the segmentations.

Segmentation type	Segmentation	Segment dimension of each foil
3	3M_Red, 3M_Blue & 3M_White	5.1 cm x 3.66 cm
4	3M_Yellow, 3M_White, 3M_Red & 3M_Blue	5.1 cm x 2.75 cm
5	Ora_Red, 3M_Blue, Ora_White, 3M_Yellow & 3M_Red	5.1 cm x 2.20 cm
6	Ora_Red, 3M_Blue, Ora_White, 3M_Yellow, 3M_Red & Ora_Yellow	5.1 cm x 1.83 cm

A naming scheme is also introduced for the rotational speed of the movement of the corresponding joint of the robotic arm. Since the maximum rotational speed of this joint is given by the vendor with 2.5 rad/s, the applied speed refers to percentages of this maximum speed. So, for example, setting the rotational speed to 100% corresponds to the maximum of 2.5 rad/s. 50 % corresponds to 1.25 rad/s and so forth. Table 3 summarizes the applied speed settings and their corresponding naming used further on.

TABLE 3. Rotational speed settings.

Speed setting	Speed in rad/s
25 %	0.625
50 %	1.25
75 %	1.875
100 %	2.5

In order to show the capabilities of the approach for sensing the movements of and communicating with robotic arms, the following experiments have been conducted:

- Comparing the achievable results of the two implemented decision trees for 3 segmentations and 4 segmentations
- Segmenting the foils placed on the robotic arm into 3 to 6 segments of different foils at a constant rotational speed of 25 % (∼0.625 rad/s).
- Increasing the rotational speed to the described distinct levels for the different segmentations.
- The impact of the sampling rate of the ADC is discussed. While for the first experiments the sample rate of the ADC is 20 Hz, it further on is increased.
- Showing the influence of a tilt of the robotic arm on the achievable results for a 3-segmentation scenario.
- After incorporating an OOK modulation scheme for LED operation, its impact on the performance of foil determination is shown.
- Finally, the performance of the approach under the presence of ambient light is discussed.

VII. RESULTS

In order to assert the correct determination of the rotation direction, the output of the decision trees alongside the timestamp and the GPIO status was stored in a text file and transferred to a standard laptop for processing and analysis in the GNU/Octave tool. In a first processing step, the text file was imported and based on the given GPIO status the different runs of the movements were separated. Each run was then processed in two filtering stages, necessary to remove the classifications done during the transition period, when one foil moves out of the detection area and the next foil is moving into the detection area. These transitions must be filtered since the classification results are invalid during this transition, because our training of the decision tree does not include the signals acquired during the passage from one foil to the next. As outlined before, the training of these transitions would be very time-consuming, since every possible combination of foils would have to be trained for the clockwise and counterclockwise rotations in such an approach. Additionally, the transition is a transient process, which is highly influenced by the rotational speed of the arm. This would result in the necessity to train all the transitions at all the different speeds. As outlined before, in our approach the training effort is aimed to be a minimum, by training only single foils without any time-dependency.

A. FILTERING

The filtering process consists of two main stages. In the first stage, all classification results that yield foils, which are not used in this particular scenario, are removed. So for example in the 3-segmented scenario, having 3M_Red, 3M_Blue and 3M_White, all classification results that differ from these three types of foils are removed. To illustrate this, Figure 11 shows the unfiltered classification results for the 3-segmented scenario over time given in incrementing numbers (x-axis), and the classification output on the y-axis. The movement was clockwise, therefore the correct sequence of foils is 3M_Red, 3M_Blue, 3M_White and 3M_Red. Since the rotation is a 350° turn, at the end of the rotation, the 3M_Red foil is again facing upward toward the VLS unit 2.0. The transition periods are highlighted with red circles.

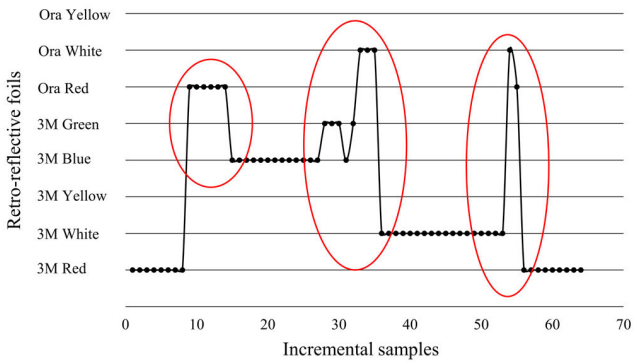

FIGURE 11. Raw results of the 3-segmented scenario with the transition periods highlighted (red circles).

As can be seen from Figure 11, at the beginning of the movement the 3M_Red foil is determined correctly. When the transition period from 3M_Red to 3M_Blue begins, the classification output is becoming invalid (leftmost red circle). When the arm has rotated further, the classification output becomes stable at the correct output of 3M_Blue, until the next transition period begins. Since the used foils in this scenario are considered to be known, we can remove all classification results that yield other foils than the described ones, such as Ora_Red, Ora_White etc.

The second stage of filtering removes non-stable classification outputs by removing classifications that are not steady for at least six consecutive classifications at a sampling rate of 20 Hz. With Figure 11, we can already show the validity of our two theorems, the one that although a movement occurs,

stable phases of detection can be achieved and second, that the transition periods can be filtered out of the sequence of determined foils.

B. DETERMINATION OF CORRECT RESULTS

After the filtering stage, each run was analyzed if the rotation direction was determined correctly. In order that a run is considered to be correct, the following specifications must be fulfilled:

- All the foils used in the scenario must be determined
- The foils must be determined in the correct sequence of the respective movement (clockwise/counterclockwise)
- The total number of transitions from one stable foil determination to the next must coincide with the number of the used foils in the scenario + 1

With these strict evaluation factors, whether the rotation direction of each run was determined correctly or not, we can substantiate that the complete rotation must be correctly determined and a single failure in determining one of the segments, causes the run to be counted as incorrect. These strict assessment criteria give reason to argue that in scenarios where not a rotation of 350° is performed, still the respective foils are determined correctly.

In the following subsection C, the achieved correct determinations are given for the implemented decision trees (raw features vs. relative features) for the two scenarios of segmentation type 3 (three segments) and segmentation type 4 (four segments).

C. COMPARISON OF RESULTS FOR RAW AND RELATIVE FEATURES

In order to determine which set of features yields better results, the achieved percentages of the correct rotation direction determinations are compared for the 3-segmentations scenario and the 4-segmentations scenario for the rotational speed of 25 %. In this setting 20 runs in total (10 clockwise/10 counterclockwise) for each segmentation type have been performed. As will be shown by the results of these experiments, the performed 20 runs are sufficient in order to give a clear statement which features outperform the others. Table 4 shows the achieved percentages of correct determinations. Please note that the decision trees have been implemented to run in parallel to guarantee an unbiased comparison.

TABLE 4. Comparison of correct determinations for raw features and relative features.

Percentage of correct rotation direction determinations		
Scenario	Raw features	Relative features
3 segments	50 %	100 %
4 segments	0 %	95 %

Table 4 shows that the utilization of relative features outperforms the classification based on raw features. Whilst the determination with relative features achieves 100% correct results for the 3-segmentations scenario and 95 % correct results for the 4-segmentations scenario, in contrast the raw features only achieve 50 % and 0 %. As anticipated during the design of our solution approach, utilizing the raw features, which are only depending on the intensity of the reflected light, is not applicable. This is because of the obvious reason that reducing the size of the reflective area of one foil will have a strong impact on the intensity of light reflected from this foil. Therefore, this approach is predestinated to fail. On the contrast, the spectral composition of the reflected light is anticipated to be stable, since, although the magnitude of the impinging light has changed due to the smaller size of reflective area of the foil, this change in magnitude is present in all the three channels equally and consequently, the relative characteristics remain stable. Based on this comparison and well founded by the shown results, we can deduce that the raw features can not be used. Consequently, we will only present the results for the relative features in the following discussions of the results.

D. RESULTS FOR DIFFERENT SEGMENTATIONS

In order to demonstrate the capabilities of our approach, we evaluated the results for the different segmentation types at the slowest applied rotational speed of 25%. With these experiments one can evaluate if our conclusions drawn in section II – Solution approach - can be verified, such as that the sequence of the foils does not have an influence on the achievable results and that the movement direction (clockwise/counterclockwise) does not have an effect on the correct determination process as well. Figure 12 shows the achieved results for the different segmentation types described in Table 2.

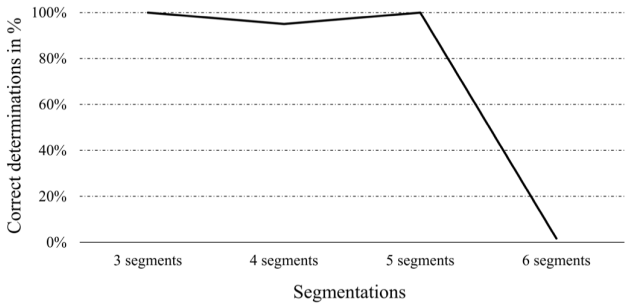

FIGURE 12. Correct determinations for different segmentations.

Figure 12 outlines that for three segments the direction of the rotational movement can be determined with 100% accuracy. For the scenario of having four different foils attached on the robotic arm, the achieved accuracy is 95 %. Increasing the number to five segments still showed the excellent result of 100 percent correct determinations. However, for a scenario with six segmentations only in 1.66 % of the performed rotations, the scenario was determined correctly.

This is because with the increase of the number of different foils, the sizes of the respective foils are decreasing

and consequently the time span the respective foil is in the spot of the LED and the detection area of the photodiode is reduced. This leads to shorter intervals between stable outputs of the classification and the transition periods described in Section A. For the 6-segmentations scenario, the effect of the transition period is overwhelming, because the time a single foil is reflecting the light towards the photodiode is minimal. These results show that our designed system fulfills the expectation that the sequences of the foils are not affecting the results negatively, regardless whether 3, 4 or 5 different foils are placed on the robotic arm.

Furthermore, since the movements were carried out in clockwise and counterclockwise directions, the results prove that the same highest accuracy can be achieved, regardless of the respective direction. The scenario of having 6-segmentations on the robotic arm shows the current limitation for our solution approach. The deterioration of the performance is due to the effect of overlapping reflections from the applied foils, caused by the decreased area size. Anyhow, up to this limit we can show that, without having to adapt the underlying algorithms, highest accuracy can be achieved in the determination of the movement direction as well as the used foils since a result is only considered as correct when the sequence of determined foils is in accordance with the actual sequence and all the used foils have been determined correctly. To put this into the perspective of a 350° rotatable arm, this means that in the scenario of having 5-segmentations, for every movement that exceeds about 70° degrees, the direction of the movement can be determined accurately.

E. INFLUENCE OF ROTATIONAL SPEED ON THE ACHIEVABLE RESULTS

Increasing the rotational speed of the robotic arm reduces the time period for which a respective foil is in the detection area of the photodiode. In the following we discuss the impact of different rotational speed settings, namely 25 %, 50 %, 75 % and 100 % (maximum) on the achieved results. Table 5 summarizes the results for correct determinations of different segmentation types for these four speed settings. Please note that in the scenarios of having 5-segmentations and 6-segmentations the experiments were done for 60 runs instead of 20 runs, since these two scenarios were anticipated to be more challenging for our system and therefore more runs would cause a better statistical evaluation for these two scenarios.

TABLE 5. Comparison of correct determinations for different rotational speeds and segmentations.

Speed settings	3 segments	4 segments	5 segments *	6 segments *
25%	100 %	95 %	100 %	1.66 %
50%	100 %	95 %	96.66 %	0 %
75%	100 %	95 %	76.66 %	0 %
100 %	100 %	100 %	56.66%	0 %

*60 runs of measurements

With the 20 runs conducted for the scenarios of three segments and four segments our system is achieving the same perfect results for all speeds. This shows that the rotational speed has no major impact when three or four segments are used, which is the main intention of these experiments, clearly deductible already after 20 runs. At higher numbers of segmentations, a negative effect on the accuracy of the determinations can be observed with increasing speed. This is because of the additional intensification of the problem related to the transition periods. Since at higher rotational speeds the time span where only one foil is present in the detection area is decreasing also the number of correct determinations decreases. For 6 segments no correct estimation can be achieved. In order to increase the correct estimation rate for the 5-segmented scenario in accordance with our solution approach, it would be necessary to enable the system to detect the stable periods of a foil detection procedure with higher accuracy. A straightforward approach to enable this is to increase the sampling rate of the ADC from 20 Hz to 1 kHz. This simple solution is set to relief this problem, since a higher number of samples will be acquired during the time span a single foil is in the detection area. It is clear that this would also result in more samples being acquired during the transition period and consequently leading to more invalid classifications, but as shown in Section A, these transition periods between two respective foils can be filtered to a large extend.

F. INCREASE OF THE SAMPLING RATE TO 1 kHz

In order to verify the assumption that a higher sampling rate would cause better results for larger numbers of segmentations, the 5-segmentations scenario was repeated with a higher sampling rate of 1 kHz. Due to our flexible system design, only the ADC control and the control mechanism to access the AXI bus registers had to be adjusted in order to enable a higher sampling rate. All the other software components including the decision trees, as well as the hardware components remained unchanged, which is one more benefit of our solution approach. Especially for time-depending training data an increase of the sampling rate would lead to the necessity of retraining the model. However, since we use only features inferred from stable reflections, we do not have to perform this time-consuming process again.

After these minor adjustments in the ADC control and the AXI bus control, overall 60 runs were conducted with the new sampling rate of 1 kHz. The achieved results are given in Table 6, where in the left column the numbers of correct determinations at 20 Hz are repeated, whilst in the right column the achieved numbers of correct determinations for 1 kHz can be found.

The comparison in Table 6 illustrates the huge improvement realizable by increasing the sampling rate. Especially at the highest applicable rotational speed of 100 %, the percentage of correct determinations can be almost doubled from 56.66% to 96.66 %. We would like to point out again that this major improvement was realized by a simple adaption

TABLE 6. Comparison of correct determinations for different rotational speeds for five segmentations at 1 kHz sample rate.

Speed settings	5 segments at 20 Hz	5 segments at 1 kHz
25%	100 %	98.33 %
50%	96.66 %	98.33 %
75%	76.66 %	91.66 %
100 %	56.66 %	96.66 %

in the ADC control and AXI bus, without the need for any other modification of the system. The results achieved with the higher sampling rate for the 5-segmentations scenario furthermore also proves the fulfillment of the requirement that the speed of the movement does not deteriorate the achievable performance of our system significantly. Another conclusion that can be drawn from these results is that, since the approach is proved to be almost unaffected by the applied speed, any movement within speed settings of 25 % to 100 % can be considered to be detected accurately.

G. INFLUENCE OF THE TILT OF THE ROBOTIC ARM

Since a perfect horizontal alignment of the robotic arm cannot be guaranteed, especially in an industrial environment where the robotic arm also has to perform actions that require the arm to tilt up and down, we evaluated the effect of a possible tilt of the robotic arm on the results. For these experiments, we applied a tilt by moving the robot arm at joint 3 in a 3-segmented scenario with the rotational speed set to 50 %. The experiments were repeated for different tilting angles with both a positive tilt as well as a negative tilt. With the tilt of 0° the robotic arm is in horizontal direction parallel to the VLS unit 2.0. A positive tilt in this regard, describes that the robotic arm is tilted toward the VLS unit 2.0, whilst a negative tilt describes a tilt away from the VLS unit 2.0. The experiments have been repeated at the distinct tilting angles of $-20°$, $-15°$, $-10°$, $-5°$, $+5°$, $+10°$, $+15°$ and $+20°$. Table 7 lists the results for the respective tilting angles and the corresponding percentages of correct determinations.

TABLE 7. Achieved correct determinations at different tilting angles.

Tilting angle in degree	Correct determinations in %
-20°	35 %
-15°	35 %
-10°	100 %
-5°	100 %
5°	100 %
10°	100 %
15°	0 %
20°	0 %

A closer look on the results of Table 7 shows that in the range from – 10° to + 10 ° tilting angles all of the performed movements for the chosen 3-segmentation scenario have been determined correctly. The comparison of the results at $-15°$ and $+15°$ shows a significant difference. The explanation why still 35% of the runs can be determined correctly when the tilt is negative, compared to no correct results for a positive tilt larger than 10°, is based on the direction of the movement. Whilst with a negative tilt (away from the VLS unit 2.0) the reflective area remains in the main beam direction of the LED, at a positive tilt the reflective area moves out of this main beam direction. Furthermore, when a positive tilt is applied, the front part of the robotic arm, since it is moved toward the VLS unit 2.0, is reflecting more light toward the photodiode and therefore affects the spectral composition of the impinging light.

With the presented results, we can show that our system, in a 3-segmentations scenario, is resilient to the application of a tilting angle between $-10°$ and $+10°$. This leads to the big advantage that even when the arm is not perfectly horizontally aligned, our solution approach proves to be valid and can therefore relieve the requirement regarding a perfect alignment of the robotic arm in relation to the receiving elements of our proposed system.

H. INCORPORATING VISIBLE LIGHT COMMUNICATION

As outlined in the introducing chapter of this work, visible light communication offers some certain advantages in the area of Industry 4.0, especially in industrial environments where bandwidth limitations or interferences between wireless RF communication methods can occur. In order to unleash the potentials of utilizing VLC in this context, it is of utter importance to guarantee the operation of both VLC and VLS functionalities in parallel without any deterioration of the performance. In this section, we will show how our system can be easily adapted to enable also visible light communication via the LED on the VLS unit 2.0, without any influence on the accuracy of movement determination.

As mentioned, in the FPGA and software implementation section, our design choice for the processing unit offers us the possibility to implement a VLC functionality, whilst the VLS task is not affected. This can be achieved by transferring the LED control from the SoC part of the Ultra96-V2 board to the FPGA part. Since the ADC control logic is already implemented in the FPGA fabric, we can now extend this particular entity to perform also the modulation of the LED in a closely time-coupled way with the ADC control. Therefore, we realized the straightforward solution that the LED/ADC control block must guarantee that the LED is on during the acquisition phase of the ADC. This however also clearly defines the time span during which VLC communication can be realized, namely when the ADC is idle. For the modulation, we choose a simple OOK modulation. The corresponding block diagram is shown in Figure 13.

The tight coupling of the ADC control with the modulation of the LED for communication purposes is shown in Figure 14, with the guaranteed ‘‘Fixed LED ON period’’ (during which the sensing task is performed) labelled as well as the time slot in which the communication can be performed. This time slot is labelled as ‘‘Modulation bits’’ (during which the sensing task is off and any desired modulation of the light can be conducted).

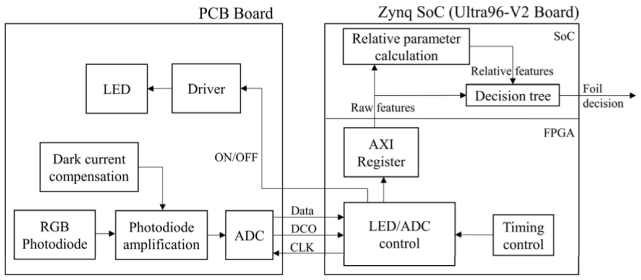

FIGURE 13. Block diagram for enabling VLC and VLS in parallel.

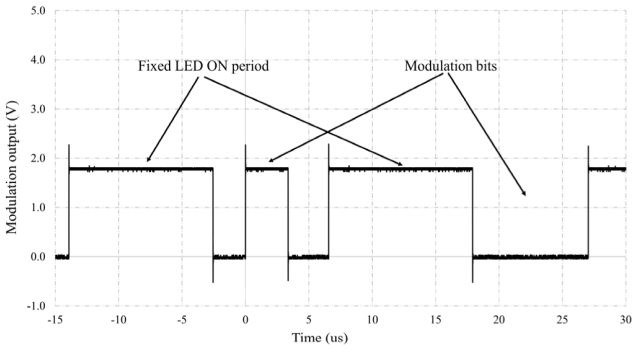

FIGURE 14. Data transmission scheme of the VLS unit 2.0.

With this time division multiplexing between the task of VLS and VLC, we can demonstrate that the combination of VLC and VLS in our designed VLS unit 2.0 is not only doable, but again can be realized with only minor adaptions of the whole system and especially there is no need for any modification of the decision trees. It is obvious that due to the implemented modulation of the LED, also the measured illuminance on the experimental setup will change, since the LED is not always on. In the presence of the modulation scheme, the illuminance measured by the handheld MK350S PREMIUM spectrometer on the area where the retroreflective foils are placed is decreasing to 160 lux, compared to the measured 265 lux without modulation.

To substantiate our anticipation that our implemented combination of VLC and VLS will not deteriorate the achievable performance we repeated the measurements with the modulation present for a 5-segmentations scenario with the before described improvement of increasing the sampling rate to 1 kHz. The measurements were done for all the four speed levels and overall 60 runs were conducted. Table 8 shows the results without modulation in the left column, whilst the right column gives the percentage values of correct determinations when the light source is modulated.

These results highlight that the combination of VLC and VLS shows the same high accuracy as the scenario without the communication task. Furthermore, two other big advantages can be realized by the modulation of the light source without any major effort. First, the results show that our solution approach is also applicable in scenarios where dimming of the light source is a requirement (the measured illumination decreased by around 100 lux for the scenario including the communication task). Second, we observed during the experiments that by modulating the light source the thermal behavior of the LED becomes better and consequently, the amount of time the VLS unit 2.0 needs to be actively cooled by the fan decreases. Yet, the biggest improvement validated by the achieved results is that the tasks of VLC and VLS can be performed in parallel without any deterioration of the accuracy. This is a big step towards the vision of utilizing visible light based technologies in parallel for communication and sensing in the area of industry 4.0.

TABLE 8. Comparison of correct determinations for different rotational speeds for five segmentations with and without a modulated light source.

Speed settings	5 segments without modulation	5 segments with modulation
25 %	98.33 %	96.66 %
50 %	98.33 %	100 %
75 %	91.66 %	100 %
100 %	96.66 %	100 %

I. INFLUENCE OF AMBIENT LIGHT

Finally, the influence of ambient light on the performance of our system is of great interest, since in the envisioned application scenario (e.g. factory setting), the complete absence of ambient light cannot be taken for granted. Unlike in the previous measurements, in the following experiments the installed fluorescent tubes in the utilized laboratory room were switched on during the online test. Please note that we did not change any parameters of the VLS unit 2.0, both in software or hardware. Especially we would like to emphasize that the decision tree established, based on training data acquired in the absence of ambient light, remains also unchanged. In order to illustrate the effect of ambient light in terms of the spectral composition of the light that impinges on the reflective surface, we used the handheld MK350S PREMIUM spectrometer to measure the respective spectra. Figure 15(a), Figure 15(b), and Figure 15(c), show the spectral compositions of the light at the surface of the reflective area for three different cases. Figure 15(a) shows the spectral composition for the case that only the CREE LED light source from the VLS unit 2.0 is on, while Figure 15(b) shows the spectral composition for the case that only the fluorescent tubes of the artificial room lighting are on. Finally, Figure 15(c) shows the spectral composition of the impinging light in case that both the LED and the fluorescent tubes are turned on.

For the demonstration of the influence of ambient light, we choose the 5-segmentations scenario. In order to obtain comparable results with the previous conducted experiments, we also performed 60 runs for the four speed settings of 25%, 50%, 75% and 100%. Table 9 shows the achieved rate of correct determinations for the conducted experiments in this regard.

On overall, we can observe that the rate of correct determinations is decreasing compared to the previous experiments with only the LED of the VLS unit 2.0 as the light source.

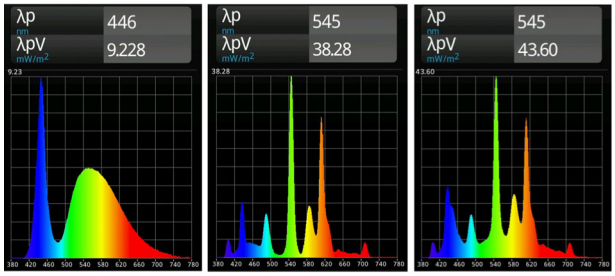

FIGURE 15. Spectral power distributions at the surface of the retroreflective foils mounted on the robotic arm: a) only the LED of the VLS unit 2.0 is on, b) only the fluorescent tubes of the artificial room lighting are on c) both LED and fluorescent tubes are on.

TABLE 9. Correct determinations for different rotational speeds for five segmentations under the presence of ambient light.

Speed settings	Correct determinations
25%	70 %
50%	83.33 %
75%	91.66 %
100 %	83.33 %

Nevertheless, even in the worst performing scenario, with the speed set to 25%, in 42 out of the 60 runs our system is able to determine not only all foils placed on the robotic arm, but also in the correct order of the movement direction. These promising results were achieved without any need to retrain the system for the new lighting conditions. Furthermore, it must be pointed out that the applied ambient light is very challenging, since a completely different type of light source (fluorescent tubes) is used for ambient lighting. This shows that the utilization of relative parameters as the features for the decision tree generation shows a high potential for visible light sensing even under the presence of ambient light.

VIII. CONCLUSION AND FUTURE WORK

In this work, we showed that the determination of the rotation direction and the rotation characteristics of a robotic arm can be achieved by only placing retroreflective foils on the robot, without the need for any kind of active sensors. The successful application of machine learning utilizing decision trees is demonstrated for this purpose, without the requirement of extensive time-consuming training of combinations of the retroreflective foils. Based on the achieved results we substantiate, that with our implemented system approach high accuracies in the determination can be achieved for various conditions such as different rotational speeds and different tilting angles, without the need for retraining. Furthermore, we showed that the usage of relative features, resembling the spectral composition of the reflected light, outperforms the usage of raw (absolute) features, depending on the intensities of the reflected light. Overall for scenarios where up to 5 different foils are placed on the robotic arm, the detection of the foils as well as the correct sequence of the foils were demonstrated to be performed with correct determination rates well above 90 %. One of the main advantages of our proposed system and the designed solution approach is that the tasks of VLS and VLC can be combined without any negative impact. This means that sensing and communication can be done in parallel with one and the same low-complexity infrastructure and without the need for active sensors and devices placed on the robotic arm (despite the need for a photodiode to be mounted on the robotic arm for the acquisition of the VLC data). Our successful combination of VLS and VLC outlines that also the integration of VLP functionalities that depend on the broadcast of data by the light source, by the means of VLC, would be possible. The combination of VLC, VLS and VLP shows the potential for future scenarios in Industry 4.0, where for example a mobile robot can accurately move to a position and then performs the task of rotation, which is accurately monitored by VLS.

Concluding our experimental investigations, we also showed that our proposed system is still operable even in case that additional artificial lighting sources are switched on. All this was achieved without the need for retraining or other major adaptions, thus rendering our proposed solution to be reliable, with the major advantages of utilizing low-complexity methods and no necessity to perform time-consuming and consequently costly training measurements.

Other contactless methods measuring rotations are in particular based on optical and magnetic sensors. Magnetic based sensors are sensing the strength of a magnetic field and usually consist of one or multiple magnet(s) mounted on the rotating device and a sensor placed in close vicinity of the rotating device. The main drawback of this method is that the magnet and the sensor have to be placed in close vicinity to each other and that an additional sensor has to be placed in the infrastructure, whilst in our approach the receiving device (RGB photodiode) can be integrated into the obligatory room lighting.

Optical based sensors that are applied in this regard range from laser diodes or LEDs to camera based systems. In comparison to our work, we showed that no additional special transmitters such as laser diodes have to be introduced, but that a common LED that in addition can be used for room lighting can be utilized for determining the rotation of the robotic arm. In general camera based systems, in comparison to our proposed solution, have higher requirements in terms of computational power to process the algorithms and furthermore camera based systems are often associated with privacy concerns.

The scenario in which 6-segmentations of different foils were used on the robotic arm, demonstrates the current limit for our solution approach. The thorough inspection of the results in the 6-segmentations scenario shows that the designed filtering stages need to be adapted in the future for these higher segmentation numbers. In future work we will pursue two approaches in order to enable higher segmentations with our system. First, we will incorporate the

known order of the segmentation into the filtering stages to determine if a transition from a stable foil classification to the next is plausible or if this transition is caused by the already explained mixture of the reflected light from different foils during the transition period. In the current filtering stages, only the knowledge if a foil is used in this scenario is applied. The second approach is to enhance the classification done by the decision tree by extending the training data to different light levels during the acquisition of the reflected light and consequently modulating the LED between these light levels also during the online phase.

Furthermore, although a correct determination of the movements failed for larger tilting angles, this also opens the possibility for further options. The measurements and results reported here in this regard were done without retraining. In more sophisticated approaches, in which the system is trained for different tilt angles, it should be therefore possible also to determine and differentiate between different tilt angles of the robot arm.

Nevertheless, the achieved results prove that the application and combination of Visible Light Sensing and Visible Light Communication can become a key player in the context of Industry 4.0. In particular, it also can be a strategy toward one of the key goals of 6G strategies, which is to amalgamate sensing, positioning and communication [47].

ACKNOWLEDGMENT

The authors would like to thank Andreas Kröpfl for supporting the experimental set-up and manuscript preparation.

REFERENCES

[1] D. Feezell and S. Nakamura, "Invention, development, and status of the blue light-emitting diode, the enabler of solid-state lighting," *Comput. Rendus Phys.*, vol. 19, no. 3, pp. 113–133, Mar. 2018.

[2] P. M. Pattison, M. Hansen, and J. Y. Tsao, "LED lighting efficacy: Status and directions," *Comput. Rendus Phys.*, vol. 19, no. 3, pp. 134–145, Mar. 2018.

[3] M. Franz and F. P. Wenzl, "Critical review on life cycle inventories and environmental assessments of LED-lamps," *Crit. Rev. Environ. Sci. Technol.*, vol. 47, no. 21, pp. 2017–2078, Nov. 2017.

[4] P. M. Pattison, J. Y. Tsao, G. C. Brainard, and B. Bugbee, "LEDs for photons, physiology and food," *Nature*, vol. 563, no. 7732, pp. 493–500, Nov. 2018.

[5] P. H. Pathak, X. Feng, P. Hu, and P. Mohapatra, "Visible light communication, networking, and sensing: A survey, potential and challenges," *IEEE Commun. Surveys Tuts.*, vol. 17, no. 4, pp. 2047–2077, 4th Quart., 2015, doi: 10.1109/COMST.2015.2476474.

[6] J. Luo, L. Fan, and H. Li, "Indoor positioning systems based on visible light communication: State of the art," *IEEE Commun. Surveys Tuts.*, vol. 19, no. 4, pp. 2871–2893, 4th Quart., 2017, doi: 10.1109/COMST.2017.2743228.

[7] H. Haas, C. Chen, and D. O'Brien, "A guide to wireless networking by light," *Prog. Quantum Electron.*, vol. 55, pp. 88–111, Sep. 2017.

[8] U. Rehman, S. Ullah, P. H. J. Chong, S. Yongchareon, and D. Komosny, "Visible light communication: A system perspective overview and challenges," *Sensors*, vol. 19, no. 5, pp. 1–22, Mar. 2019.

[9] A. B. M. M. Rahman, T. Li, and Y. Wang, "Recent advances in indoor localization via visible lights: A survey," *Sensors*, vol. 20, no. 5, p. 1382, Mar. 2020.

[10] O. Ergul, E. Dinc, and O. B. Akan, "Communicate to illuminate: State-of-the-art and research challenges for visible light communications," *Phys. Commun.*, vol. 17, pp. 72–85, 2015.

[11] L. U. Khan, "Visible light communication: Applications, architecture, standardization and research challenges," *Digit. Commun. Netw.*, vol. 3, no. 2, pp. 78–88, May 2016, doi: 10.1016/j.dcan.2016.07.004.

[12] M. F. Keskin, A. D. Sezer, and S. Gezici, "Localization via visible light systems," *Proc. IEEE*, vol. 106, no. 6, pp. 1063–1088, Jun. 2018.

[13] Q. Wang and M. Zuniga, "Passive visible light networks: Taxonomy and opportunities," in *Proc. Workshop Light Up IoT*, 2020, pp. 42–47, doi: 10.1145/3412449.3412551.

[14] W. Wang, Q. Wang, J. Zhang, and M. Zuniga, "PassiveVLP: Leveraging smart lights for passive positioning," *ACM Trans. Internet Things*, vol. 1, no. 1, pp. 1–24, Mar. 2020, doi: 10.1145/3362123.

[15] R. Raj, K. Saxena, and A. Dixit, "Passive optical identifiers for VLC-based indoor positioning systems: Design, hardware simulation, and performance analysis," *IEEE Syst. J.*, vol. 15, no. 3, pp. 3208–3219, Sep. 2021, doi: 10.1109/JSYST.2020.3002585.

[16] K. Deprez, S. Bastiaens, L. Martens, W. Joseph, and D. Plets, "Passive visible light detection of humans," *Sensors*, vol. 20, no. 7, p. 1902, Mar. 2020, doi: 10.3390/s20071902.

[17] A. P. Weiss, S. Z. Rad, and F. P. Wenzl, "Pose detection with backscattered visible light sensing utilizing a single RGB photodiode: A model based feasibility study," *Proc. Int. Wireless Commun. Mobile Comput. (IWCMC)*, Limassol, Cyprus, 2020, pp. 137–142, doi: 10.1109/IWCMC48107.2020.9148177.

[18] Y. Yang, J. Hao, J. Luo, and S. J. Pan, "CeilingSee: Device-free occupancy inference through lighting infrastructure based LED sensing," in *Proc. IEEE Int. Conf. Pervas. Comput. Commun. (PerCom)*, Kona, HI, USA, Mar. 2017, pp. 247–256, doi: 10.1109/PERCOM.2017.7917871.

[19] D. Kaholokula, "Reusing ambient light to recognize hand gestures," Dartmouth Comput. Sci., Hanover, NH, USA, Tech. Rep. TR2016-797, 2016.

[20] L. Yu, H. Abuella, M. Z. Islam, J. F. O'Hara, C. Crick, and S. Ekin, "Gesture recognition using reflected visible and infrared lightwave signals," *IEEE Trans. Human-Mach. Syst.*, vol. 51, no. 1, pp. 44–55, Feb. 2021, doi: 10.1109/THMS.2020.3043302.

[21] H. Abuella and S. Ekin, "Non-contact vital signs monitoring through visible light sensing," *IEEE Sensors J.*, vol. 20, no. 7, pp. 3859–3870, Apr. 2020, doi: 10.1109/JSEN.2019.2960194.

[22] Y. Almadani, D. Plets, S. Bastiaens, W. Joseph, M. Ijaz, Z. Ghassemlooy, and S. Rajbhandari, "Visible light communications for industrial applications—Challenges and potentials," *Electronics*, vol. 9, no. 12, p. 2157, Dec. 2020, doi: 10.3390/electronics9122157.

[23] E. W. Lam and T. D. C. Little, "Visible light positioning for location-based services in industry 4.0," in *Proc. 16th Int. Symp. Wireless Commun. Syst. (ISWCS)*, Aug. 2019, pp. 345–350.

[24] G. Aceto, V. Persico, and A. Pescape, "A survey on information and communication technologies for industry 4.0: State-of-the-art, taxonomies, perspectives, and challenges," *IEEE Commun. Surveys Tuts.*, vol. 21, no. 4, pp. 3467–3501, 4th Quart., 2019, doi: 10.1109/COMST.2019.2938259.

[25] B. Turan, K. A. Demir, B. Soner, and S. C. Ergen, "Visible light communications in industrial Internet of Things (IIOT)," in *The Internet of Things in the Industrial Sector Computer Communication and Networks*, Z. Mahmood, Ed. Cham, Switzerland: Springer, 2019, pp. 163–191.

[26] P. W. Berenguer, D. Schulz, J. Hilt, P. Hellwig, G. Kleinpeter, J. K. Fischer, and V. Jungnickel, "Optical wireless MIMO experiments in an industrial environment," *IEEE J. Sel. Areas Commun.*, vol. 36, no. 1, pp. 185–193, Jan. 2018, doi: 10.1109/JSAC.2017.2774618.

[27] H. Yang, A. Alphones, W. Zhong, C. Chen, and X. Xie, "Learning-based energy-efficient resource management by heterogeneous RF/VLC for ultra-reliable low-latency industrial IoT networks," *IEEE Trans. Ind. Informat.*, vol. 16, no. 8, pp. 5565–5576, Aug. 2020, doi: 10.1109/TII.2019.2933867.

[28] H. Yang, W.-D. Zhong, C. Chen, and A. Alphones, "Integration of visible light communication and positioning within 5G networks for Internet of Things," *IEEE Netw.*, vol. 34, no. 5, pp. 134–140, Sep. 2020, doi: 10.1109/MNET.011.1900567.

[29] *International Telecommunication Union*, document ITU-R SM.2422-0, Jun. 2018. Accessed: Aug. 30, 2021. [Online]. Available: https://www.itu.int/dms_pub/itu-r/opb/rep/R-REP-SM.2422-2018-PDF-E.pdf

[30] (Jan. 2020). *3M, 3M Diamond Grade DG3 Reflective Sheeting Series 4000*. Accessed: Aug. 30, 2021. [Online]. Available: https://multimedia.3m.com/mws/media/349914O/pb-4000-3m-diamond-grade-dg3-reflective-sheeting.pdf

[31] *ORAFOL Europe GmbH, ORALITE VC 170 Universal Film Technical Datasheet 2016/31*. Accessed: Aug. 30, 2021. [Online]. Available: https://www.orafol.com/products/europe/en/technical-data-sheet/oralite-vc-170-universal-film-8674-technical-data-sheet-europe-en.pdf
[32] I. A. Bustoni, I. Hidayatulloh, A. M. Ningtyas, A. Purwaningsih, and S. N. Azhari, "Classification methods performance on human activity recognition," *J. Phys., Conf. Ser.*, vol. 1456, Oct. 2020, Art. no. 012027.
[33] T. Zebin, P. J. Scully, and K. B. Ozanyan, "Evaluation of supervised classification algorithms for human activity recognition with inertial sensors," in *Proc. IEEE SENSORS*, Glasgow, U.K., Apr. 2017, pp. 1–3, doi: 10.1109/ICSENS.2017.8234222.
[34] A. S. A. Sukor, A. Zakaria, and N. A. Rahim, "Activity recognition using accelerometer sensor and machine learning classifiers," in *Proc. IEEE 14th Int. Floquium Signal Process. Appl. (CSPA)*, Penang, Malaysia, May 2018, pp. 233–238, doi: 10.1109/CSPA.2018.8368718.
[35] A. P. Weiss, K. Madane, S. Z. Rad, and F. P. Wenzl, "Implementation of a cost-efficient passive visible light sensing approach for the determination of surface colors," in *Proc. Austrochip Workshop Microelectron. (Austrochip)*, Vienna, Austria, 2019, pp. 81–86, doi: 10.1109/Austrochip.2019.00026.
[36] AVNET. *Product Brief, LIT# 5365-PB-AES-ULTRA96-V2-G-V1*. Accessed: Aug. 30, 2021. [Online]. Available: http://zedboard.org/sites/default/files/product_briefs/5354-pb-ultra96-v3b.pdf
[37] AVNET. *Ultra96-V2 Single Board Computer Hardware User's Guide Version 1.1*. Accessed: Aug. 30, 2021. [Online]. Available: http://zedboard.org/sites/default/files/documentations/Ultra96-V2-HW-User-Guide-v1_1.pdf
[38] Cree. *Product Family Data Sheet*. Accessed: Aug. 30, 2021. [Online]. Available: https://www.cree.com/led-components/media/documents/XLampMCE.pdf
[39] *Efficient Power Conversion Corporation*. Accessed: May 2020. [Online]. Available: https://epc-co.com/epc/Portals/0/epc/documents/datasheets/EPC2040_datasheet.pdf
[40] Texas Instruments. (Oct. 2018). *LMG1020 Datasheet*. Accessed: Aug. 30, 2021. [Online]. Available: https://www.ti.com/lit/ds/symlink/lmg1020.pdf?ts=1611622474654&ref_url=https%253A%252F%252Fwww.ti.com%252Fpower-management%252Fgate-drivers%252Fgan-fet-driver.html
[41] Kingbright. (Jan. 2019). *APS5130PD7C-P22 RGB Color Sensor Datasheet, V.5*. Accessed: Aug. 30, 2021. [Online]. Available: https://www.kingbrightusa.com/images/catalog/SPEC/APS5130PD7C-P22.pdf
[42] Linear Technology Corporation. *LTC6268-10/LTC6269-10 Datasheet*. Accessed: Aug. 30, 2021. [Online]. Available: https://www.analog.com/media/en/technical-documentation/data-sheets/626810f.pdf
[43] Analog Devices. (Mar. 2020). *LTC6228/LTC6229 Datasheet*. Accessed: Aug. 30, 2021. [Online]. Available: https://www.analog.com/media/en/technical-documentation/data-sheets/LTC6228-6229.pdf
[44] Linear Technology Corporation. *LTC2387-16 Datasheet*. Accessed: Aug. 30, 2021. [Online]. Available: https://www.analog.com/media/en/technical-documentation/data-sheets/238716f.pdf
[45] I. H. Witten, E. Frank, M. A. Hall, and C. J. Pal, "Appendix B—The WEKA workbench," in *Data Mining*. Burlington, MA, USA: Morgan Kaufmann, 2017, pp. 553–571, doi: 10.1016/B978-0-12-804291-5.00024-6.
[46] Niryo SAS. (Mar. 9, 2019). *Niryo One User Manual*. Accessed: Aug. 30, 2021. [Online]. Available: https://niryo.com/docs/niryo-one/user-manual/complete-user-manual/
[47] J. R. Bhat and S. A. Alqahtani, "6G ecosystem: Current status and future perspective," *IEEE Access*, vol. 9, pp. 43134–43167, 2021, doi: 10.1109/ACCESS.2021.3054833.

KUSHAL MADANE received the bachelor's degree in electronics and telecommunications from Dr. Babasaheb Ambedkar Technological University, Lonere, India, in 2011, and the master's degree in advanced electronic engineering from FH Joanneum, Kapfenberg, Austria, in 2018. He is currently pursuing the Ph.D. degree with Graz University of Technology.

Since 2018, he has been a member of the Smart Connected Lighting Group, JOANNEUM RESEARCH Forschungsgesellschaft mbH, Pinkafeld, Austria.

ANDREAS PETER WEISS received the master's degree in telematics from Graz University of Technology, in 2008, and the Ph.D. degree from the Alpen-Adria University of Klagenfurt, in 2012.

From 2012 to 2018, he worked in the field of research and development of digital circuit design, signal processing, and algorithm design. Since 2018, he has been a member of the Smart Connected Lighting Group, JOANNEUM RESEARCH Forschungsgesellschaft mbH, Pinkafeld, Austria. His research interests include visible light sensing, visible light positioning, sensors, sensor fusion, and algorithm design.

STEFAN SCHANTL was born in Vorau, Styria, Austria, in 1980. He graduated in electrical engineering, open-loop, and control engineering from HTL Pinkafeld, in 1999.

From 2000 to 2003, he worked as a hardware engineer in developing digital video displays, based on full-color RGB-LEDs. After this, he worked more than ten years as an electronic engineer on developing different consumer electronics (control systems, cashless systems, and LED display systems). Then, he started to work as an electronic engineer (research and development) for LED headlamp systems in the automotive field for more than four years. Since 2019, he has been a member of the Smart Connected Lighting Group, JOANNEUM RESEARCH Forschungsgesellschaft mbH, Pinkafeld, and is responsible for electronic development.

ERICH LEITGEB (Member, IEEE) received the master's degree from Graz University of Technology, in 1994, and the Ph.D. degree (Hons.) in February 1999. From 1982 to 1984, he attended the military service, including a training to become an Officer for communications in the Austrian army, and he is still active as an Expert in military communications (current military rank: Lieutenant-Colonel). In 1994, he started research in optical communications at the Department of Communications and Wave Propagation, Graz University of Technology. Since January 2000, he has been the project leader of international research projects in the field of optical communications. He has established and leads the Research Group for Optical Communications, Graz University of Technology, and joined several international projects (such as COST 270, the EU project SatNEx and SatNEx 2, COST 291, COST IC0802, and IC1101; currently, he participates in MP1401, CA15127, and CA16220) and ESA projects in different functions. Since 2011, he has been a Professor of optical communications and wireless applications with the Institute of Microwave and Photonic Engineering, Graz University of Technology. He is the author or coauthor of seven book chapters, over 50 journal publications, 150 peer-reviewed conference papers, over 45 invited talks, and more than 70 international scientific reports.

FRANZ PETER WENZL studied physics at Graz University of Technology, Austria, where he finished his Ph.D. thesis on organic light-emitting diodes and light-emitting electrochemical cells at the Institute of Solid State Physics, in 2004. In the following, he joined the Institute of Surface Technologies and Photonics, JOANNEUM RESEARCH Forschungsgesellschaft mbH, Weiz, Austria, where he was the Head of the research group Light and Optical Technologies, till 2018. In 2018, he started to establish a new research group of JOANNEUM RESEARCH Forschungsgesellschaft mbH on Smart Connected Lighting in Pinkafeld, Austria. His main research interests include solid state lighting, lighting engineering, color conversion, optics, visible light communication, visible light positioning, visible light sensing, and integrative lighting.